International Journal of Nanomedicine

Dovepress
Taylor & Francis Group

Open Access Full Text Article

ORIGINAL RESEARCH

Biomimetic Nanoplatform Based on the Neutrophil Membrane for Targeted Therapy of Spinal Cord Injury

Yinghui Shang[1], Wei Wang[2], Tehan Zhang[1], Enlin Qi[2], Ruizhi Jiang[2], Haiting Liu[3], Qinghai Wang[4]*, Shiqing Feng[1,*]

[1]Department of Orthopaedics, the Second Qilu Hospital of Shandong University, Shandong University Centre for Orthopaedics, Shandong University, Jinan, Shandong, 250033, People's Republic of China; [2]Department of Orthopaedics, Qilu Hospital of Shandong University, Shandong University Centre for Orthopaedics, Shandong University, Jinan, Shandong, 250012, People's Republic of China; [3]Department of Blood Transfusion, Third Xiangya Hospital, Central South University, Changsha, Hunan, 410000, People's Republic of China; [4]Department of Cardiology, the Second Qilu Hospital of Shandong University, Shandong University, Jinan, Shandong, 250033, People's Republic of China

*These authors contributed equally to this work

Correspondence: Qinghai Wang, Department of Cardiology, the Second Qilu Hospital of Shandong University, Shandong University, Jinan, 250033, People's Republic of China, Email sdwqh1005@126.com; Shiqing Feng, Department of Orthopaedics, the Second Qilu Hospital of Shandong University, Shandong University Centre for Orthopaedics, Shandong University, Jinan, 250033, People's Republic of China, Email shiqingfeng@sdu.edu.cn

Introduction: Spinal cord injury (SCI) triggers a cascade of secondary damage, including oxidative stress and neuroinflammation, for which effective treatments remain limited. To address this, we developed a biomimetic nanoplatform, NEU@MPBNPs-HED, consisting of mesoporous Prussian blue nanoparticles (MPBNPs) loaded with hederagenin (HED) and cloaked with neutrophil membranes (NEUm) to enhance lesion targeting and immune evasion.

Methods: The physicochemical properties, drug release characteristics, and cellular uptake of NEU@MPBNPs-HED were characterized. Therapeutic efficacy was evaluated in vitro using oxygen-glucose deprivation/reoxygenation (OGD/R) models of neuronal injury and in vivo in a murine spinal cord contusion model. Key outcomes included neuronal survival, oxidative stress, apoptosis, motor recovery, and biodistribution.

Results: In vitro, NEU@MPBNPs-HED significantly improved HT22 neuronal viability by 48.6%, reduced intracellular reactive oxygen species (ROS) by 52.4%, and preserved mitochondrial membrane potential compared with free HED or non-biomimetic controls. Apoptosis was suppressed through modulation of Bax, Bcl-2, and cytochrome C. In vivo, NEU@MPBNPs-HED enhanced Basso Mouse Scale (BMS) scores, improved motor evoked potentials, promoted axonal regeneration (NF200↑), and reduced glial scarring (GFAP↓). Moreover, the oxidative stress marker (MDA), inflammatory indicators (TNF-α, and Ly6G+ cells, and Arg1) were reduced. Biodistribution studies confirmed selective accumulation at the injury site, and histological analyses revealed no systemic toxicity.

Conclusion: The NEU@MPBNPs-HED nanoplatform effectively targeted spinal cord lesions, attenuated oxidative and inflammatory damage, and promoted neurological recovery. These findings highlight the translational potential of biomimetic nanotherapies for treating traumatic central nervous system disorders.

Keywords: spinal cord injury, neutrophil membrane, mesoporous Prussian blue nanoparticles, hederagenin, apoptosis

Introduction

Spinal cord injury (SCI) is a catastrophic neurological disorder that results in permanent motor, sensory, and autonomic dysfunction, profoundly impairing patients' quality of life.[1] Although surgical decompression, spinal stabilization,[2] and pharmacological agents such as methylprednisolone have been applied,[3] and pharmacological agents such as methylprednisolone have been applied. In particular, the use of high-dose methylprednisolone remains controversial due to its

Received: 16 June 2025
Accepted: 7 November 2025
Published: 24 November 2025

marginal benefit and significant side effects, despite FDA approval.[4] Therefore, the development of safe, effective, and targeted therapies for SCI remains a critical clinical priority.

Following the primary mechanical insult, SCI triggers a complex secondary injury cascade involving ischemia, hypoxia, oxidative stress, and neuroinflammation.[5,6] Among the earliest immune responders, neutrophils infiltrate the injured spinal cord within hours and can remain active for up to 10 days.[7] Their recruitment is driven by chemokines, complement proteins, leukotriene B4, and extracellular matrix degradation products.[8] This migration is primarily mediated by cell adhesion molecules such as P-selectin.[9–11] However, in addition to their innate immune functions, neutrophils also release cytotoxic mediators—including reactive oxygen species (ROS), elastase, and matrix metalloproteinases—that exacerbate tissue damage.[1] Notably, the neutrophil membrane retains its injury-homing ability without releasing intracellular pro-inflammatory contents, making it a promising tool for targeted drug delivery in SCI.

As oxidative stress and inflammation are key drivers of secondary injury, strategies that simultaneously address both processes hold significant therapeutic potential.[12] Nanotechnology-based approaches have shown promise in modulating the pathological microenvironment of SCI by scavenging ROS and attenuating inflammatory responses.[13–18] For instance, a rapamycin-loaded hollow mesoporous Prussian blue nanozyme, modified with a cell-penetrating peptide, has demonstrated dual antioxidative and anti-inflammatory functions and led to functional recovery in SCI models.[12] Similarly, Prussian blue nanocubes have been used as imaging and therapeutic agents to facilitate stem cell therapy for SCI.[19]

Hederagenin (HED), a naturally occurring pentacyclic triterpenoid saponin extracted from various herbs, exhibits broad biological activities, including anti-inflammatory, anti-lipid peroxidation, anti-cancer, and neuroprotective effects.[20,21] Previous studies have demonstrated that HED can inhibit inflammation-associated signaling pathways, reduce the production of inflammatory cytokines,[22,23] and exert neuroprotective effects in ischemic stroke models.[13] Notably, HED has been shown to attenuate sepsis-induced lung injury by suppressing NF-κB-mediated inflammation and modulating macrophage polarization.[23] Although its application in SCI has not yet been explored, these findings suggest its potential utility in neural tissue repair.

Based on these insights, we developed a biomimetic nanoplatform composed of mesoporous Prussian blue nanoparticles (MPBNPs) loaded with HED and camouflaged with neutrophil membrane vesicles (NEUm). This study investigates the targeting capability, anti-apoptotic effect, and therapeutic efficacy of this platform—termed NEU@MPBNPs-HED—in both in vitro and in vivo models of SCI (Figure 1).

Materials and Methods

Materials

Mesoporous Prussian blue nanoparticles (MPBNPs) were obtained from XFNANO Materials Technology. HED was provided by Nanjing Spring & Autumn Biological Engineering Co., Ltd. Rodamine B (RhB) was from Shanghai Aladdin Biochemical Technology Co., Ltd. Lipopolysaccharides (LPS, from E. coli 0111:B4) and rhodamine 123 (Rh123) were from Shanghai Yuanye Bio-Technology Co., Ltd. Distearoyl phosphatidyl ethanolamine-fluorescein isothiocyanate (DSPE-FITC) was from Xi'an Ruixi Biotechnology Co., Ltd. The mouse peripheral blood neutrophil isolation kit was sourced from Tianjin Haoyang Biotechnology Co., Ltd. Dialysis membranes (2 kDa) was supplied by Shanghai Gifted High Nine Trading Co., Ltd. Cy5 was supplied by Solarbio Life Technology Co., Ltd, and polycarbonate porous membrane syringe filter (200 nm) was from Shanghai Limin Industrial Co., Ltd. Thermo Fisher Technologies Co., Ltd provided trypsin, phosphate buffer solution (PBS), fetal bovine serum (FBS), glucose-free Dulbecco's modified Eagle medium (DMEM), and high-glucose DMEM were obtained from Thermo Fisher Scientific. The Cell Counting Kit-8 (CCK-8) was from Dojindo Laboratories. Annexin V-FITC/PI Apoptosis Detection and ROS Assay Kits were from Beyotime Biotechnology Co., Ltd. Antioxidant capacity kit (DPPH method) was from Meilian Biotechnology Co., Ltd. Primary antibodies for β-actin, Caspase-9, Caspase-3, Bax, Bcl-2, Cytochrome C, CD86, CD206, Neun, GFAP, NF200, MDA, TNF-α, CD68, Ly6G, iNOS and Arg1 were provided by Cell Signaling Technology Co., Ltd. Hematoxylin and eosin (H&E), horseradish peroxidase (HRP)-conjugated goat anti-rabbit and rabbit anti-mouse secondary antibodies, along with Cy3-linked, 555-linked, and 488-linked goat anti-rabbit secondary antibodies, Hoechst 33342, and DAPI were provided by Servicebio Technology Co., Ltd.

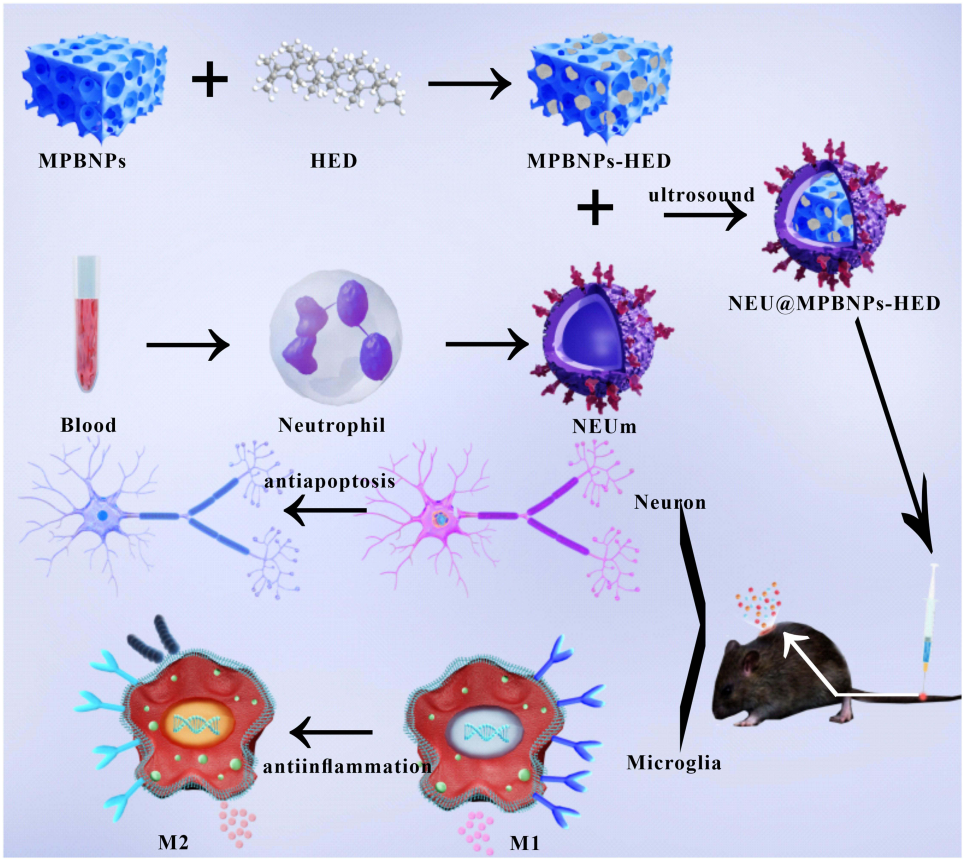

Figure 1 Schematic diagram of NEU@MPBNPs-HED construction and its application as a targeted and effective therapeutic for attenuating spinal cord injury.

Cells and Mice

Our study exclusively examined female mice. It is unknown whether the findings are relevant for male mice. RAW264.7, HT22, and BV-2 cells from Procell Life Science and Technology Co., Ltd were cultured in high-glucose DMEM supplemented with 10% FBS and 1% penicillin/streptomycin under standard conditions (37 °C, 5% CO_2, humidified atmosphere). All cell lines were authenticated and confirmed to be free of mycoplasma contamination through routine PCR-based testing prior to experimentation.

Female C57 BL/6J mice (8 weeks old) were purchased from Jinan Xingkang Laboratory Animal Technology Co., Ltd. All animal procedures were approved by the Institutional Animal Care and Use Committee (IACUC) of The Second Qilu Hospital of Shandong University (Approval No. KYLL2024550) and conducted in compliance with the animal welfare guidelines as stipulated in the institutional guidelines (Directive 2010/63/EU in Europe) for the care and use of animals.

LPS Treatment

BV-2 cells were seeded in 6-well plates at a density of 1×10^6 cells/well and treated with LPS (1.0 μg/mL) for 24 hours to induce an inflammatory response. After stimulation, cells were treated with PBS, NEUm, MPBNPs, NEU@MPBNPs, HED, MPBNPs-HED, and NEU@MPBNPs-HED. PBS-treated cells served as negative controls, and sham cells (without LPS) served as baseline controls.

Oxygen Glucose Deprivation/Reoxygenation (OGD/R) Treatment

HT22 cells were seeded at 5×10^4 cells/well in 24-well plates and incubated in glucose-free DMEM in a hypoxic chamber (1% O_2, 5% CO_2, 94% N_2) at 37 °Cfor 90 minutes. For reoxygenation, cells were cultured in high-glucose DMEM under normoxic conditions for 24 hours. Subsequently, cells were treated with PBS, NEUm, HED, MPBNPs,

https://doi.org/10.2147/IJN.S547401

NEU@MPBNPs, MPBNPs-HED, or NEU@MPBNPs-HED. PBS-treated cells served as injury controls, and sham cells were cultured in normal conditions throughout.

Spinal Cord Injury Model

Female C57 BL/6J mice were anesthetized with isoflurane, and an incision was made in the lower thoracic region of the back to expose the spine, followed by dorsal laminectomy at the T9 level. After fixing the spine, a moderate contusive spinal cord injury (70 kD force) was induced using the Infinite Horizon Impactor (PSI, USA). The muscles and skin were then sutured. Sham mice underwent similar procedures without spinal cord impact.

Preparation of Neutrophil Membrane (NEUm) Nanovesicles

Neutrophils were isolated from the whole blood of female C57 BL/6J mice using the Percoll gradient method. Activated neutrophils were obtained by treating with LPS (0.1 mg/mL) for 4 hours. Plasma membrane was isolated as described by Pilchler et al, weighed and stored at −80°C.

Preparation of MPBNPs-HED

3 mg HED and 3 mg MPBNPs were mixed in 2 mL PBS and stirred for 24 hours. After dialysis using a 2 kDa membrane to remove unloaded HED, the post-dialysis samples were collected to determine HED concentration. Encapsulation efficiency (EE) and loading efficiency (LE) were calculated.

Construction of NEU@MPBNPs-HED

Equal volumes of NEUm nanovesicles and MPBNPs-HED were fused by ultrasound and passed through a syringe filter (200 nm) 20 times. Free NEUm was removed by centrifugation (2500 rpm, 10 minutes) to obtain NEU@MPBNPs-HED.

Characterization of NEU@MPBNPs-HED

Transmission electron microscopy (TEM) was applied to evaluate the size and encapsulation of nanoparticles. Surface charge was determined using a Zetasizer Nano ZS. UV–vis spectrometry (ScanDrop) was used to detect NEU@MPBNPs-HED absorbance.

Release Property of HED in NEU@MPBNPs-HED

To verify the characteristics of pH response release, HED release from NEU@MPBNPs-HED was assessed in PBS at pH 7.4 and pH 5.4. Samples (1 mL) were dialyzed in 20 mL PBS at 37°C. HED release was quantified by measuring absorbance at 405 nm.

NEU@MPBNPs Biocompatibility

To evaluate the biocompatibility, we calculated their hemolysis rate and observed the phagocytosis activity of macrophage. Different concentrations of NEU@MPBNPs or MPBNPs blended with 5% red blood cell (RBC) suspensions were incubated at 37°C for 2 hours, and then centrifuged. Absorbance of supernatants was measured at 545 nm, and hemolysis ratio was calculated.

To evaluate macrophage phagocytosis capacity, RhB-conjugated NEU@MPBNPs or MPBNPs were co-cultured with RAW264.7 cells and then observed by laser confocal fluorescence microscopy (LCFM) after stained with Hoechst 33342.

Evaluation of the Injury Repair Effects of NEU@MPBNPs-HED in vitro

Targeting Property Assessment In Vitro

DSPE-FITC-labeled NEUm were cocultured with OGD/R-pretreated or untreated HT22 cells for 8 hours. And then fluorescence signals were observed under LCFM.

Injury Repair Effects Assessed by CCK-8

OGD/R-pretreated HT22 cells were treated with PBS, NEUm, HED, MPBNPs, NEU@MPBNPs, MPBNPs-HED, or NEU@MPBNPs-HED (HED concentration: 2.0 μg/mL) for 24 hours. The cell viability was assessed based on the protocol of CCK-8.

Apoptosis Assessment

OGD/R-pretreated HT22 cells were treated as above, and then stained with Annexin V-FITC/PI to assess cell apoptosis under LCFM.

Mitochondrial Membrane Potential (MMP) Assessment

HT22 cells were treated as above, stained with Rh123, and observed under LCFM.

Reactive Oxygen Species (ROS) Assessment

HT22 cells were treated as above, and stained according to the protocol of ROS Assay Kit, followed by observation under LCFM.

Free Radical Scavenging Assayed by DPPH Method

HT22 cells were treated as above, and processed in accordance with the instructions of the DPPH kit. The absorbance value (A) at 515 nm was measured, and the clearance rate was calculated according to the formula: Clearance rate (%) = $(1-(A_{sample}-A_{blank})/A_{control})\times 100\%$.

Immunoblot Assay

Protein extracts were quantified, and β-actin, Caspase-3, Caspase-9, Bax, Bcl-2, Cytochrome C, CD86, and CD206 protein levels were analyzed by immunoblotting.

NEU@MPBNPs-HED Distribution Assessment in vivo

After SCI, C57 BL/6J mice were administered Cy5-labeled NEU@MPBNPs or Cy5-conjugated MPBNPs. At 24 hours, spinal cords, brains, and visceral organs were collected, and fluorescence signals were analyzed using Xenogen IVIS Lumina XR imaging system. Spinal cord sections were observed by LCFM.

NEU@MPBNPs-HED Treatment in SCI Mice

After randomization, the mice were treated with PBS, NEUm, HED, MPBNPs, NEU@MPBNPs, MPBNPs-HED, or NEU@MPBNPs-HED. Evaluations were conducted on day 14 using Basso Mouse Scale (BMS) scores, catwalk gait analysis, and electrophysiological analysis. Tissues were collected, fixed, and processed for further analyses.

BMS Score Assessment

Motor function was assessed by two trained researchers on days 1, 7, and 14. Scores ranged from 0 (complete paralysis) to 9 (normal).

Catwalk Gait Assessment

On day 14, Catwalk gait analysis evaluated gait differences, with parameters automatically calculated by the analysis software.

Electrophysiological Analysis

Motor evoked potential (MEP) was recorded on day 14 using an electrophysiological device to assess nerve conduction recovery.

Neun, GFAP, and NF200 Immunofluorescence Assays

Spinal cord sections were stained for Neun, GFAP, NF200, and DAPI, and then observed under LCFM for fluorescence signal analysis. Immunofluorescence staining of spinal cord sections was conducted at 14 days post-injury, a timepoint chosen because it corresponds to the subacute phase of SCI, when neuronal loss, astrocytic activation, and axonal remodeling are clearly detectable.

MDA, TNF-α, Ly6G$^+$, CD68$^+$, iNOS and Arg1 Immunofluorescence Assays

Spinal cord sections were stained for MDA, TNF-α, Ly6G$^+$, CD68$^+$, iNOS and Arg1 according to the standard protocol of immunofluorescence staining, and then observed under LCFM for fluorescence signal analysis.

Statistic Analysis

Data were presented as mean ± SD, and SPSS 20.0 (IBM Corp., Armonk, NY, USA) was applied for statistical analysis. Univariate analysis of variance was applied for evaluating the difference between groups, and Tukey posterior tests were conducted (*$p < 0.05$, **$p < 0.01$, ***$p < 0.001$, ****$p < 0.0001$).

Results

Physicochemical Characterization and Drug Release Properties of NEU@MPBNPs-HED

The NEU@MPBNPs-HED nanocomposite was prepared by first loading HED into mesoporous Prussian blue nanoparticles (MPBNPs) to form MPBNPs-HED, which was then encapsulated into neutrophil membrane (NEUm) nanovesicles (Figure 1). As shown in Figure 2A, transmission electron microscopy (TEM) revealed the characteristic cubic morphology of MPBNPs and the vesicular structure of NEUm, with the final NEU@MPBNPs exhibiting a distinct core–shell configuration. SDS-PAGE analysis further confirmed the retention of membrane proteins after fusion, indicating that the coating process preserved NEUm components (Figure 2B).

Dynamic light scattering (DLS) and zeta potential measurements showed that the average hydrodynamic diameter of NEU@MPBNPs (~196 nm) was slightly increased compared to MPBNPs, while the surface charge shifted from –20.4 ± 7.6 mV (MPBNPs) to –29.6 ± 4.7 mV, closely matching the NEUm vesicles (–28.9 ± 5.5 mV), as shown in Figure 2C and D. These results suggest successful membrane coating and charge modification consistent with NEUm properties.

UV–vis spectroscopy analysis confirmed the coexistence of characteristic absorption peaks of MPBNPs (710 nm) and HED (405 nm) in the composite. In addition, a strong absorption band was observed near 200 nm, which likely reflects contributions from both MPBNPs and NEUm components. Therefore, while this peak suggests the presence of NEUm in

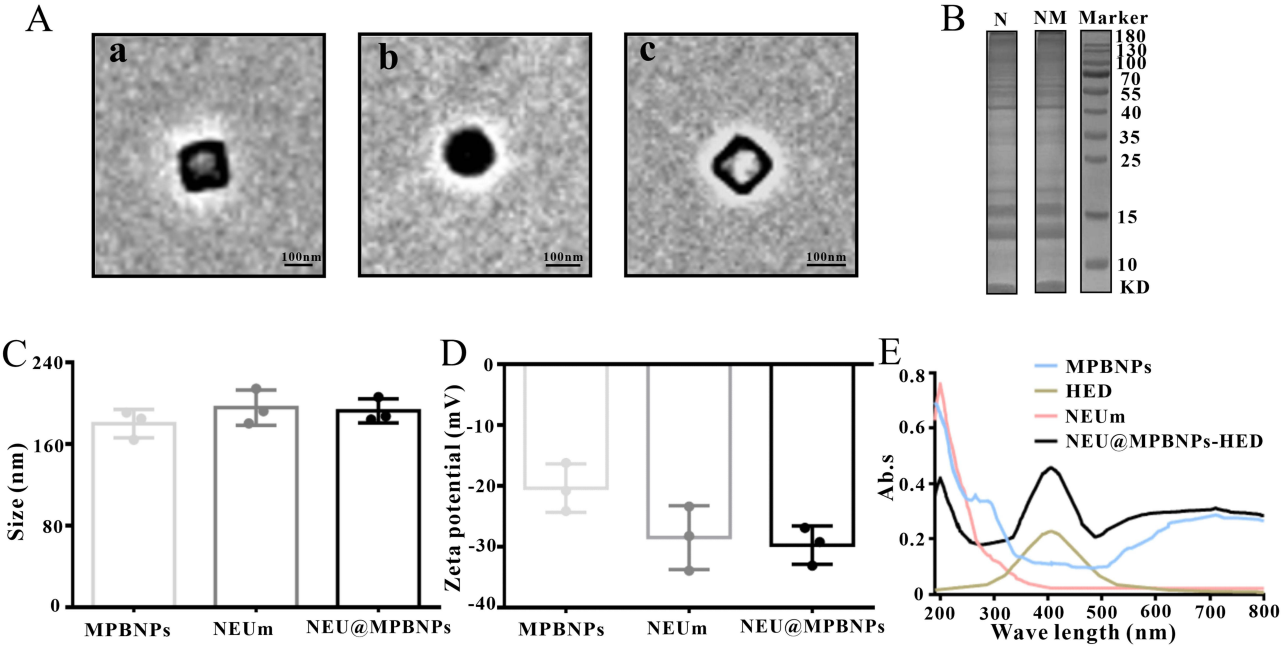

Figure 2 Characterization of NEU@MPBNPs-HED. (**A**) TEM images of (**a**) MPBNPs, (**b**) NEUm vesicles, and (**c**) NEUm-vesicle-camouflaged MPBNPs. Scale bar: 100 nm. (**B**) SDS-PAGE protein assessment. N, NEUm, NM, NEU@MPBNPs. (**C**) Particle sizes and (**D**) zeta potential values of MPBNPs, NEUm vesicles, and NEU@MPBNPs. Data are mean ± SD (n = 3). (**E**) UV–vis spectra of HED, MPBNPs, NEUm vesicles, and NEU@MPBNPs-HED.

NEU@MPBNPs-HED, we acknowledge that it may also include background absorption from MPBNPs. Taken together with the SDS-PAGE protein profiling results, these findings support the successful construction of the nanocomposite (Figure 2E).

Encapsulation efficiency (EE) and loading efficiency (LE) of HED reached 83.5 ± 4.9% and 70.3 ± 4.8%, respectively (Figure 3A), which are considerably higher than most reported nanoparticle-based systems. Furthermore, pH-responsive drug release was evaluated in PBS at pH 7.4 and 5.4, simulating physiological and acidic inflammatory microenvironments. As shown in Figure 3B, significantly more HED was released at pH 5.4 (90.4% over 48 h), compared to neutral pH (56.2%), indicating enhanced drug release under acidic conditions—a favorable feature for spinal cord injury therapy.

Biocompatibility of NEU@MPBNPs

Biocompatibility indicators, such as hemolysis and phagocytosis, are key factors that limit the applicability of nanomaterials in clinical settings,[24] so we evaluated the biocompatibility of NEU@MPBNPs through hemolysis and phagocytosis assays. To assess hemocompatibility, red blood cells (RBCs) were treated with MPBNPs and NEU@MPBNPs, and hemolysis was measured. Neither MPBNPs nor NEU@MPBNPs led to obvious hemolysis (Figure 4A), with hemolysis ratio for MPBNPs (2.0 mg/mL) being below 2% and hemolysis rate of NEU@MPBNPs being lower (Figure 4B), indicating that NEU@MPBNPs had better hemocompatibility and biosafety.

To evaluate the anti-phagocytosis capability, RhB-labeled MPBNPs or NEU@MPBNPs were co-cultured with RAW264.7 macrophages for 24 hours. As shown in Figure 4C, MPBNPs-RhB treated macrophages showed strong green fluorescence, indicating significant phagocytosis of MPBNPs. Under the same conditions, NEU@MPBNPs-RhB-treated macrophages showed significantly weaker fluorescence, suggesting reduced phagocytosis. The average fluorescence intensity in NEU@MPBNPs-RhB-treated macrophages was significantly lower than that in MPBNPs-RhB-treated cells (Figure 4D). These results indicate that NEUm encapsulation reduced macrophage-mediated clearance. Overall, NEU@MPBNPs demonstrated superior biocompatibility.

Vitro Anti-Injury Effects of NEU@MPBNPs-HED

Targeting Property of NEUm in vitro

To assess the in vitro therapeutic potential of NEU@MPBNPs-HED, HT22 cells subjected to OGD/R insult were used. As shown in Figure 5A, DSPE-FITC-labeled NEUm vesicles exhibited stronger accumulation in OGD/R-treated cells than in untreated cells, confirming enhanced targeting of injured neurons.

Cell viability assays (Figure 5B) revealed that treatment with MPBNPs, NEU@MPBNPs, and NEU@MPBNPs-HED significantly improved cell survival compared to the PBS control, with NEU@MPBNPs-HED showing the highest viability. NEUm alone did not induce a statistically significant effect.

Apoptosis, evaluated by Annexin V-FITC/PI staining (Figure 5C and F), was reduced in the HED, MPBNPs-HED, and NEU@MPBNPs-HED groups, with the latter showing the most pronounced effect.

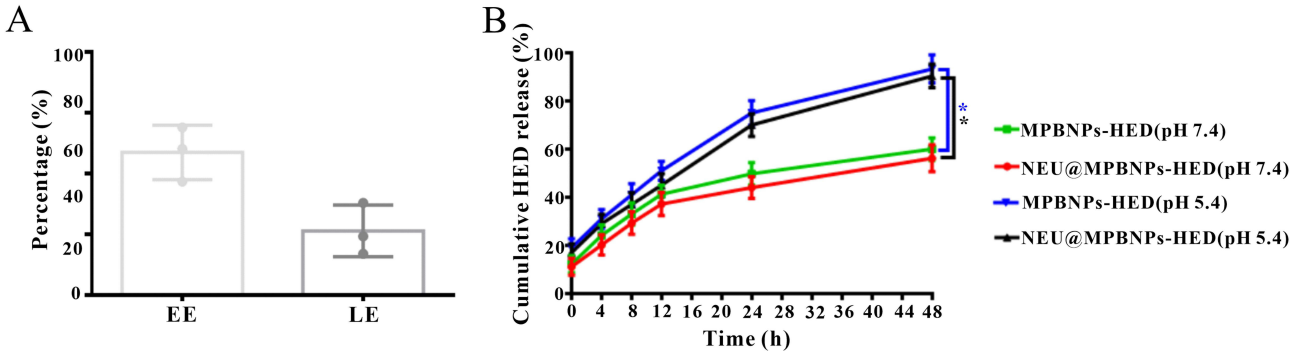

Figure 3 Drug LE of MPBNPs and release rate of NEU@MPBNPs-HED. (**A**) EE and LE of MPBNPs. (**B**) Cumulative release rates of HED from NEU@MPBNPs-HED or MPBNPs-HED at different pH values (5.4 and 7.4). Data are mean ± SD (n = 3). Comparison between groups: * $p < 0.05$.

https://doi.org/10.2147/IJN.S547401

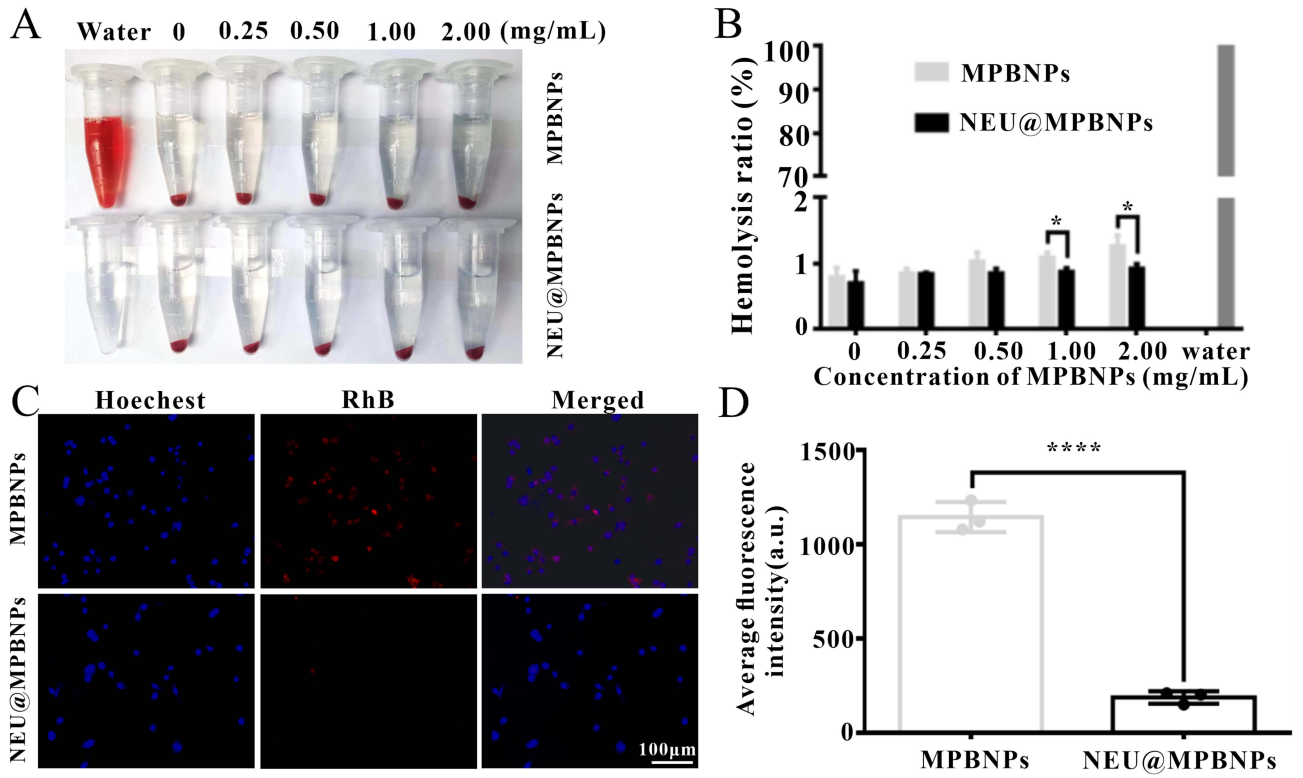

Figure 4 Biocompatibility of NEU@MPBNPs. (**A**) Images of RBC suspensions after treatment with different amounts of MPBNPs and NEU@MPBNPs. (**B**) Hemolytic ratios upon treatment with different amounts of MPBNPs and NEU@MPBNPs. Data are mean ± SD (n = 3). Compared to the MPBNPs group: * $p < 0.05$. (**C**) LCFM images of RAW264.7 cells upon culture with MPBNPs-RhB or NEU@MPBNPs-RhB for 24 h. Scale bar: 100 μm. (**D**) Average fluorescence intensities of RAW264.7 after co-culture with MPBNPs-RhB or NEU@MPBNPs-RhB for 24 h. Data are mean ± SD (n = 3). Compared to the MPBNPs group: **** $p < 0.0001$.

Mitochondrial membrane potential (MMP), assessed by Rh123 staining (Figure 5D and F), was better preserved in the NEU@MPBNPs-HED group, indicated by decreased fluorescent signal loss.ROS levels, detected using a fluorescent probe (Figure 5E and F), were significantly decreased following treatment with NEU@MPBNPs-HED compared to other treatment groups.

As shown in Figure 5G, MPBNPs perform a good free radical clearance rate (19.84% ±2.795), while NEU@MPBNPs-HED possess the best eliminating rate (51.29%± 1.286), indicating that the nanocomposite demonstrated superior free radical scavenging activity.

Expression Levels of Apoptosis- and Inflammation-Related Proteins

We evaluate the levels of apoptosis-related proteins in HT22 cells and the level of inflammatory markers in BV-2 cells to further elucidate the mechanisms underlying the anti-injury effect of NEU@MPBNPs-HED. Apoptosis is strongly correlated to the activation of caspases, which are classified as promoters (such as Caspase-9) and performers (such as Caspase-3).[25] Treatment with NEU@MPBNPs-HED, MPBNPs-HED, or HED led to decreased Caspase-9. As depicted in Figure 6A–C, compared with the control group, the expressions of Caspase-9 and Caspase-3 decreased after treatment with NEU@MPBNPs-HED, MPBNPs-HED or HED, and both of them decreased most significantly in the NEU@MPBNPs-HED group, indicating the strongest anti-apoptosis effect. The discharge of mitochondrial proteins (such as Cytochrome C) is dependent on the MMP, which is highly controlled by the Bcl-2 protein family, such as Bax and Bcl-2.[26] Bax can promote apoptosis though oligomerization at the mitochondrial surface to decrease the MMP, while Bcl-2 has the opposite effect.[27,28] The release of Cytochrome C facilitates the formation of apoptosis bodies and caspase activation.[29] As shown in Figure 6A–C, Bax and Cytochrome C decreased, and Bcl-2 expression increased after treatment with NEU@MPBNPs-HED, MPBNPs-HED or HED.

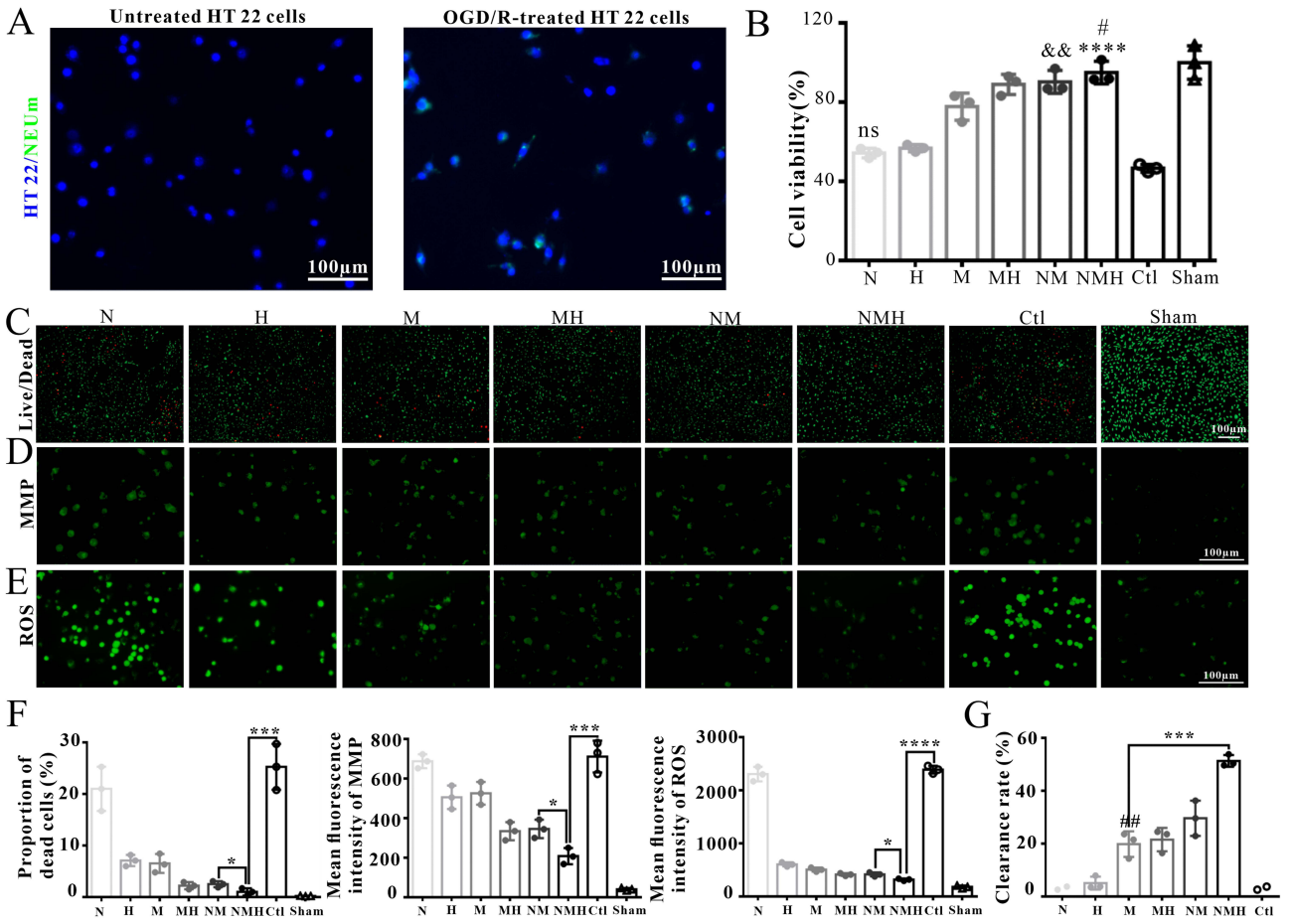

Figure 5 In vitro anti-damage efficiency of NEU@MPBNPs-HED. N, NEUm; H, HED; M, MPBNPs; MH, MPBNPs-HED; NM, NEU@MPBNPs; NMH, NEU@MPBNPs-HED; Ctl, control. (**A**) LCFM image of HT22 cells (a) or OGD/R-treated HT22 cells (b) after coculture with DSPE-FITC-labeled NEUm vesicles for 8 h. Scale bar: 100 μm. (**B**) OGD/R-treated HT22 cells viability upon administration of PBS, NEUm, HED, MPBNPs, NEU@MPBNPs, MPBNPs-HED, and NEU@MPBNPs-HED for 24 h. Data are mean ± SD (n = 3). Compared to the control group: ns, not significant, **** $p < 0.0001$; compared to the MPBNPs group: $^{\&\&}$ $p < 0.01$; compared to the MPBNPs-HED group: $^{\#}$ $p < 0.05$. (**C**) Apoptosis assessed by fluorescence microscope in OGD/R treated HT22 cells administered with PBS, NEUm, HED, MPBNPs, NEU@MPBNPs, MPBNPs-HED, and NEU@MPBNPs-HED for 24 h. Scale bar: 100 μm. (**D**) MMP assessment by fluorescence microscope in OGD/R-treated HT22 cells after administered with PBS, NEUm, HED, MPBNPs, NEU@MPBNPs, MPBNPs-HED, and NEU@MPBNPs-HED for 24 h. Scale bar: 100 μm. (**E**) ROS level evaluation by fluorescence microscope in OGD/R-treated HT22 cells after administered with PBS, NEUm, HED, MPBNPs, NEU@MPBNPs, MPBNPs-HED, and NEU@MPBNPs-HED for 24 h. Scale bar: 100 μm. ((**F**) Statistical analysis of proportion of dead cells, MMP and ROS. Intergroup comparison: * $p < 0.05$, *** $p < 0.001$, and **** $p < 0.0001$. (**G**) Free radical clearance rate assessed by DPPH method in OGD/R-treated HT22 cells after administered with PBS, NEUm, HED, MPBNPs, NEU@MPBNPs, MPBNPs-HED, and NEU@MPBNPs-HED for 24 h. Data are mean ± SD (n = 3). Compared to the control group: $^{\#\#}$ $p < 0.01$; compared to the MPBNPs group: *** $p < 0.001$.

Inflammatory reactions usually lead to a series of secondary insults after SCI, thus inhibition of inflammation at the early stage can provide a good environment for SCI repair.[30] CD86 is the cell surface marker of M1-polarized (pro-inflammatory) microglia, and CD206 is the membrane protein of M2-related (anti-inflammatory) microglia.[31] NEU@MPBNPs-HED inhibited the expression of proinflammatory marker CD86, while increased the expression level of anti-inflammatory marker CD206 (Figure 6B and C), suggesting effective modulation of inflammation.

Vivo Distribution of NEU@MPBNPs

To evaluate the in vivo therapeutic potential and targeting efficiency of NEU@MPBNPs-HED, Cy5-labeled NEU@MPBNPs or MPBNPs were administered to SCI mice. Fluorescence imaging at 24 hours post-injection revealed significantly stronger accumulation of NEU@MPBNPs in the injured spinal cord compared to MPBNPs, with reduced distribution in non-target organs such as the liver, kidney, and brain (Figure 7A–C), indicating enhanced lesion-specific targeting. This result was further validated by fluorescence intensity analysis of DAPI-stained spinal cord sections, which showed significantly higher Cy5 signal in the NEU@MPBNPs group (Figure 7D and E).

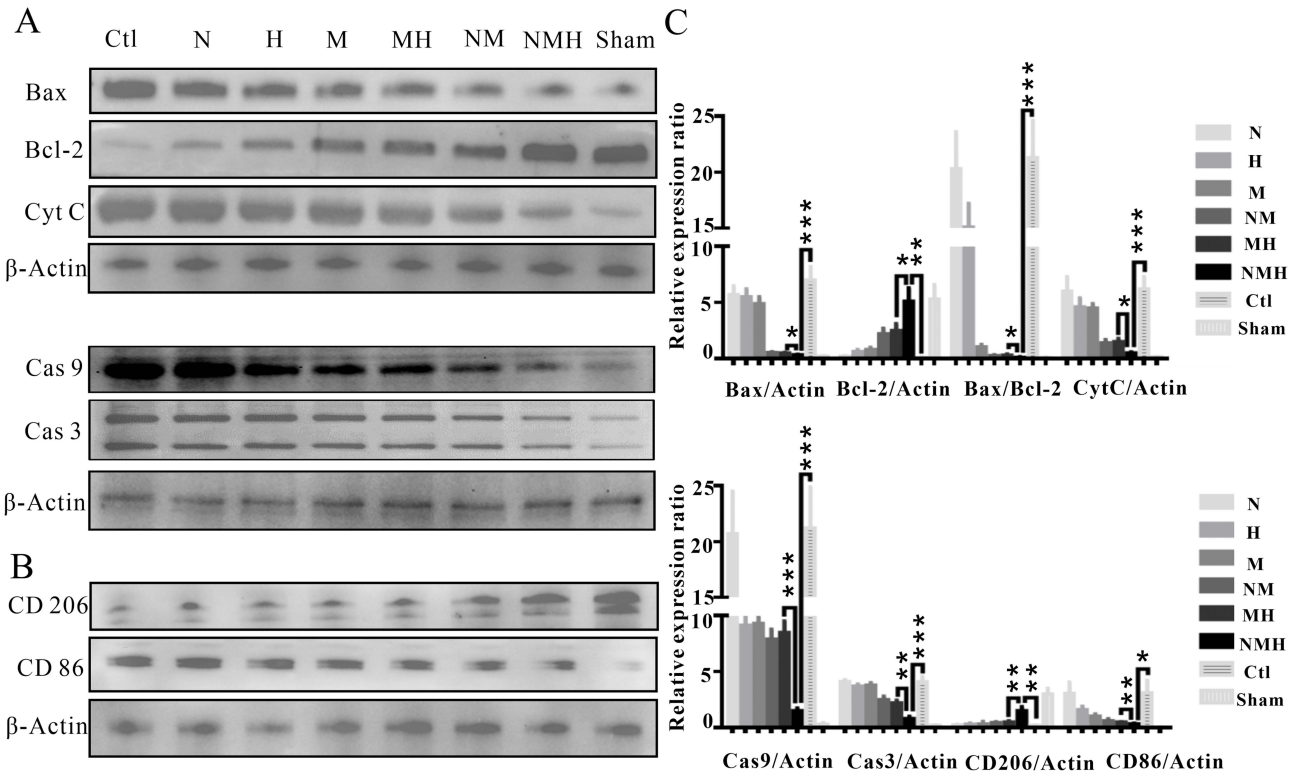

Figure 6 Immunoblot analysis of apoptosis-related and inflammatory-associated proteins. Ctl, control; N, NEUm; H, HED; M, MPBNPs; MH, MPBNPs-HED; NM, NEU@MPBNPs; NMH, NEU@MPBNPs-HED. (**A**) Expression amounts of apoptosis-related proteins in HT22 cells at 24 h after treatment with PBS, NEUm, HED, MPBNPs, NEU@MPBNPs, MPBNPs-HED, and NEU@MPBNPs-HED. (**B**) Expression amounts of CD86 and CD206 in BV-2 cells at 24 h after treatment with PBS, NEUm, HED, MPBNPs, NEU@MPBNPs, MPBNPs-HED, and NEU@MPBNPs-HED. (**C**) Relative expression ration of related proteins. Intergroup comparison: * $p < 0.05$, ** $p < 0.01$, and *** $p < 0.001$.

Subsequently, the functional efficacy of NEU@MPBNPs-HED was assessed using Basso Mouse Scale (BMS) scoring, CatWalk gait analysis, motor evoked potentials (MEPs), and immunofluorescence staining of Neun, GFAP, and NF200. These comprehensive evaluations confirmed the neuroprotective and regenerative effects of the treatment in vivo.

BMS Score Analysis

BMS score was used to assess behavioral recovery.[32] Compared to the control and NEUm groups, mice treated with HED, MPBNPs, and NEU@MPBNPs-HED showed improved BMS scores, with the NEU@MPBNPs-HED group demonstrating significantly higher scores compared to the MPBNPs-HED group (Figure 8A), indicating enhanced motor recovery.

Catwalk gait analysis was performed to evaluate hindlimb function recovery.[33] Regularity index describes the exclusive use of normal step sequence patterns during uninterrupted locomotion.[33] Max intensity at % is the time in seconds since the start of a run that the maximum intensity is measured. Max intensity at % is relative to the stand of a paw.[33] As shown in Figure 8B and C, NEU@MPBNPs-treated mice demonstrated better gait parameters compared to MPBNPs-treated mice, and NEU@MPBNPs-HED-treated mice showed significant improvement in gait compared to MPBNPs-HED-treated mice, further supporting the effectiveness of NEUm encapsulation.

Electrophysiological and Histological Assessment of Neural Recovery

MEPs recordings were conducted to assess nerve conduction recovery.[34] NEU@MPBNPs-HED-treated mice exhibited larger MEP amplitudes compared to MPBNPs-HED-treated mice (Figure 9A and B), indicating better recovery of nerve conduction function.

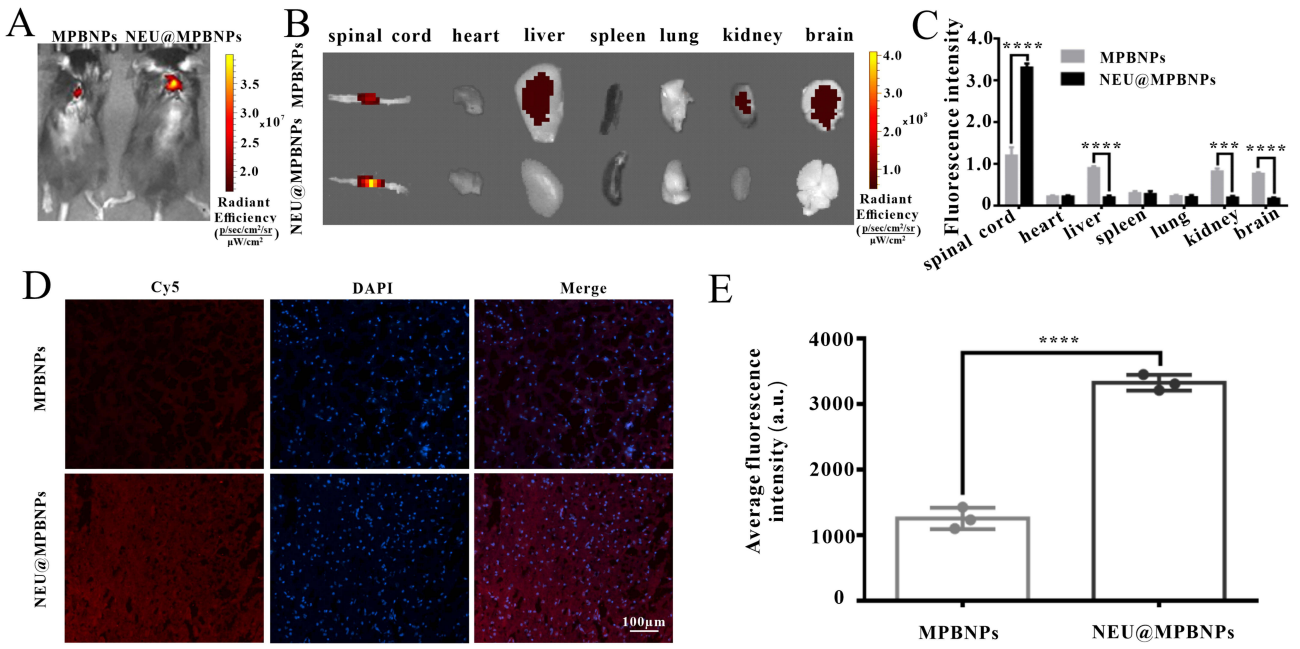

Figure 7 In vivo targeting potential of NEU@MPBNPs-HED. (**A**) Bioluminescence images of mice at 24 h of post-treatment with Cy5-conjugated MPBNPs and Cy5-linked NEU@MPBNPs. (**B**) Ex vivo bioluminescence images of visceral organs and spinal cords at 24 h of post-treatment with Cy5-conjugated MPBNPs and Cy5-linked NEU@MPBNPs. (**C**) Semiquantitative assessment of fluorescence signals of spinal cord and other tissue specimens. Data are mean ± SD (n = 3). Compared to the MPBNPs group: *** $p < 0.001$, and **** $p < 0.0001$. (**D**) Fluorescence imaging of spinal cord tissues from mice at 24 h after administration of Cy5-linked MPBNPs and Cy5-conjugated NEU@MPBNPs. Scale bar: 100 μm. (**E**) Semiquantitative assessment of fluorescence signals of spinal cord sections after DAPI staining. Data are mean ± SD (n = 3). Compared to the MPBNPs group: **** $p < 0.0001$.

Neun protein is a well-known neuron marker to investigate neuronal changes.[35] Immunofluorescence analysis of spinal cord sections showed increased green fluorescence for Neun in the NEU@MPBNPs-HED group, indicating enhanced neuron recovery (Figure 10A). NF200 is a neurofilament protein involved in axonal sprouting.[36] The green fluorescence intensity of NF200 was also strongest in the NEU@MPBNPs-HED group, suggesting better recovery of axonal sprouting (Figure 10B). Additionally, the red fluorescence intensity of GFAP was weakest in the NEU@MPBNPs-HED group, indicating reduced glial scarring and improved neuronal recovery.

Antioxidative and Antiinflammation Effect Evaluated by Immunofluorescence Staining

Immunofluorescence staining further confirmed the antioxidative and anti-inflammatory effects of NEU@MPBNPs-HED in spinal cord tissue. MDA (malondialdehyde) is a commonly used indicator of membrane lipid peroxidation, which reflects the degree of intracellular oxidative stress. MDA fluorescence was significantly reduced (Figure 11A), consistent with decreased ROS and enhanced radical scavenging observed in Figure 5E–G. CD68 levels showed no obvious change, while TNF-α expression was markedly decreased (Figure 11B). Moreover, iNOS (M1 marker) showed no significant variation, whereas Arg1 (M2 marker) expression was reduced, and Ly6G fluorescence was also diminished after NEU@MPBNPs-HED treatment (Figure 11C). These results indicate that NEU@MPBNPs-HED effectively attenuates oxidative stress and modulates macrophage-associated inflammatory responses at the tissue level.

Adverse Effect Evaluation by Histological Assay

Histological evaluation based on the H&E-stained sections of major organs, including hearts, livers, spleens, lungs, and kidneys, revealed no abnormalities in any of the treatment groups, including PBS, NEUm, MPBNPs, NEU@MPBNPs, HED, MPBNPs-HED, and NEU@MPBNPs-HED (Figure 12). These results indicate that NEU@MPBNPs-HED and related treatments were safe and did not cause adverse effects.

https://doi.org/10.2147/IJN.S547401

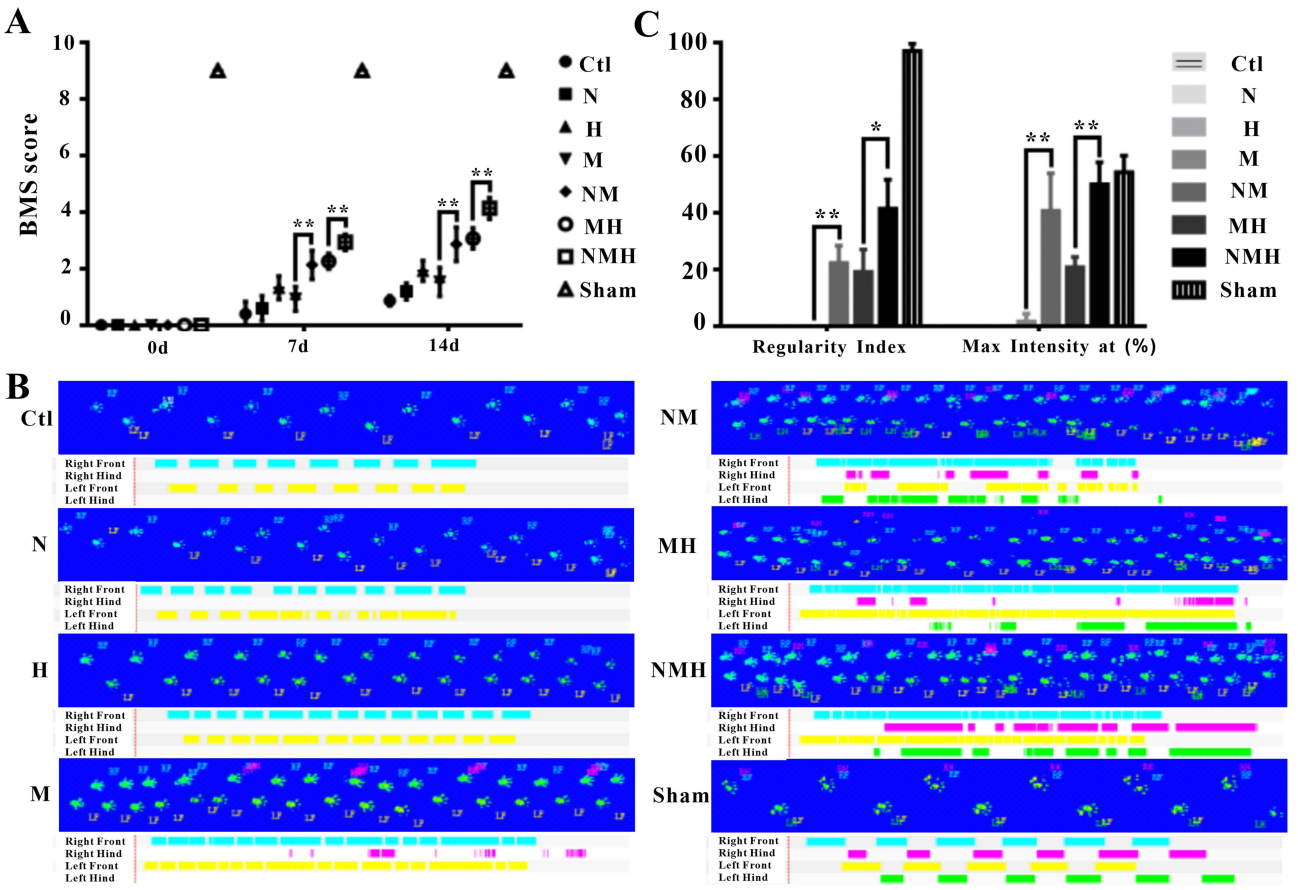

Figure 8 BMS Score and Catwalk Gait of mice after treatment with NEU@MPBNPs-HED. Ctl, control; N, NEUm; H, HED; M, MPBNPs; NM, NEU@MPBNPs; MH, MPBNPs-HED; NMH, NEU@MPBNPs-HED. (**A**) BMS Score of the injured mice 14 days after intravenous injection of PBS, NEUm, HED, MPBNPs, NEU@MPBNPs, MPBNPs-HED, and NEU@MPBNPs-HED. Data are mean ± SD (n=3). Comparison between groups: ** $p<0.01$. (**B**) Catwalk Gait of the injured mice 14 days after intravenous injection of PBS, NEUm, HED, MPBNPs, NEU@MPBNPs, MPBNPs-HED, and NEU@MPBNPs-HED. (**C**) Statistic analysis of Regularity index and Max intensity at %. Data are mean ± SD (n=3). Comparison between groups: * $p<0.05$, ** $p<0.01$.

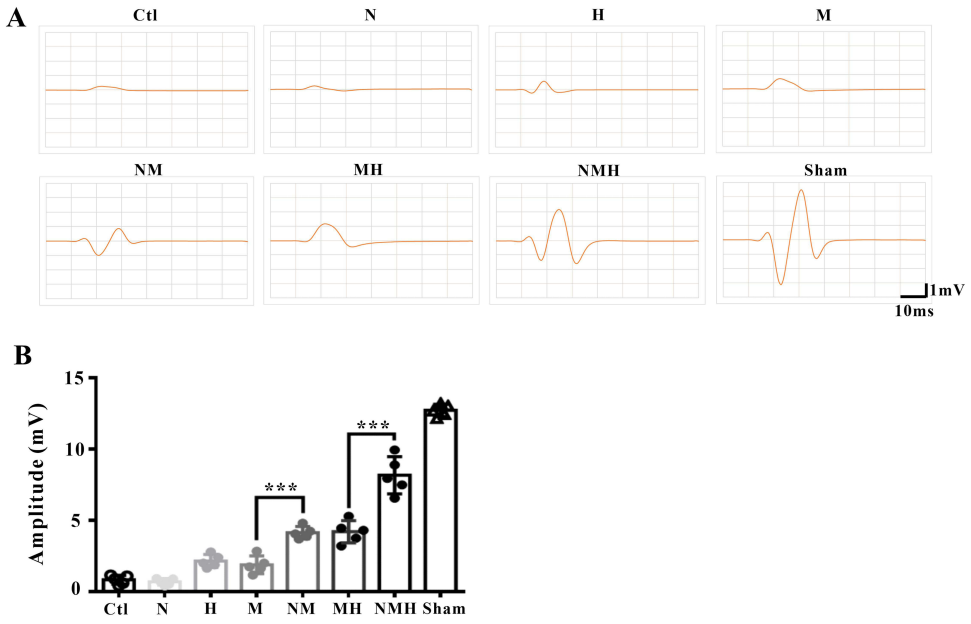

Figure 9 MEP analysis of the injured mice 14 days after intravenous injection of PBS, NEUm, HED, MPBNPs, NEU@MPBNPs, MPBNPs-HED, and NEU@MPBNPs-HED. Ctl, control; N, NEUm; H, HED; M, MPBNPs; NM, NEU@MPBNPs; MH, MPBNPs-HED; NMH, NEU@MPBNPs-HED. (**A**) Recorded MEP of the injured mice. (**B**) Statistic analysis of the amplitude of MEP. Data are mean ± SD (n=3). Comparison between groups: *** $p<0.001$.

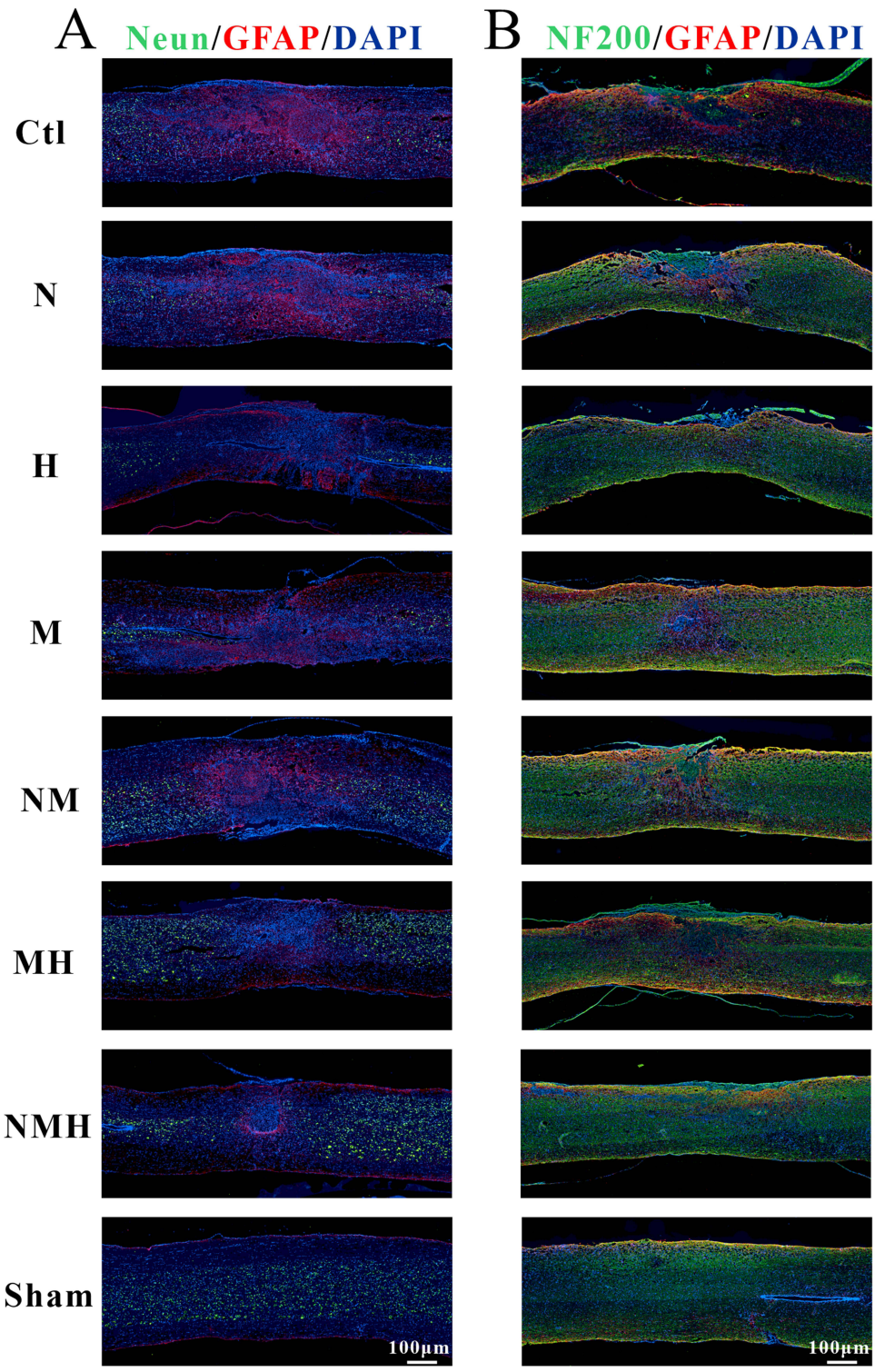

Figure 10 Neun, GFAP, and NF200 immunofluorescence staining of the damaged spinal cord tissues. Ctl, control; N, NEUm; H, HED; M, MPBNPs; NM, NEU@MPBNPs; MH, MPBNPs-HED; NMH, NEU@MPBNPs-HED. Neun and GFAP (**A**), and NF200 and GFAP (**B**) assays assessing spinal cord injury at 14 days after intravenous injection of PBS, NEUm, HED, MPBNPs, NEU@MPBNPs, MPBNPs-HED, and NEU@MPBNPs-HED. Scale bar: 100 μm.

Discussion

This study reveals that NEU@MPBNPs-HED, a neutrophil membrane-coated nanoplatform co-delivering HED and MPBNPs, effectively targets the spinal cord lesion and promotes neuroprotection in both in vitro and in vivo SCI models. Compared with previously reported nanotherapies focusing on either anti-inflammatory[12] or antioxidant functions,[13,18]

https://doi.org/10.2147/IJN.S547401

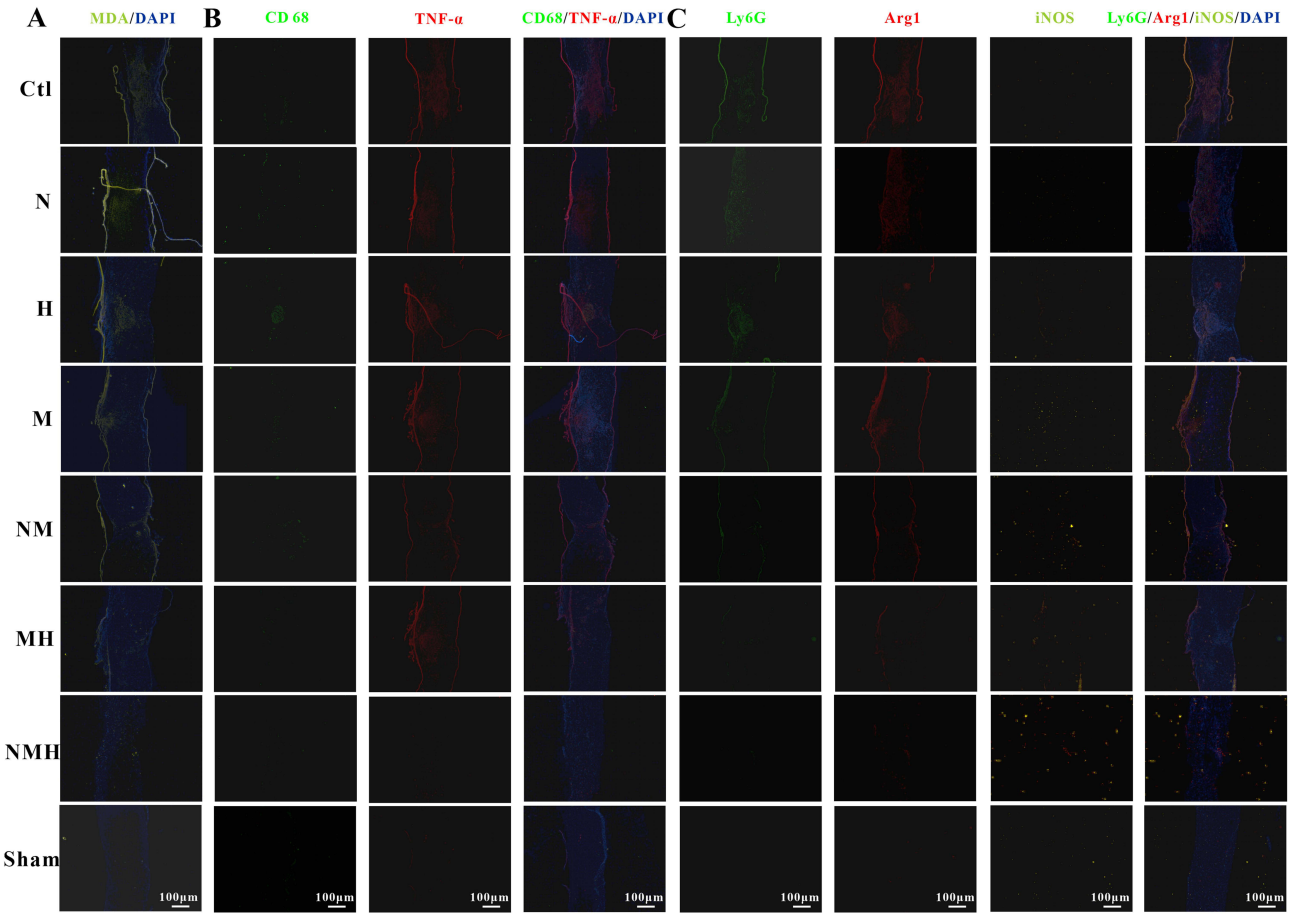

Figure 11 (**A**) MDA, (**B**) TNF-α and CD68, and (**C**) Ly6G, iNOS and Arg1 immunofluorescence staining of the damaged spinal cord tissues at 14 days after intravenous injection of PBS, NEUm, HED, MPBNPs, NEU@MPBNPs, MPBNPs-HED, and NEU@MPBNPs-HED. Ctl, control; N, NEUm; H, HED; M, MPBNPs; NM, NEU@MPBNPs; MH, MPBNPs-HED; NMH, NEU@MPBNPs-HED. Scale bar: 100 μm.

this dual-functional system achieves improved therapeutic outcomes through synergistic suppression of ROS, apoptosis, and neuroinflammation.

Mechanistically, NEU@MPBNPs-HED significantly reduced ROS levels and preserved mitochondrial membrane potential, which corresponded with decreased expression of Caspase-3/9, Bax, and Cytochrome C, and upregulation of Bcl-2. These effects align with earlier findings on HED's modulation of mitochondrial apoptosis and NF-κB signaling in ischemic models.[18,23] The neutrophil membrane coating further enhanced delivery selectivity to the injured spinal cord, a feature not commonly utilized in prior SCI-targeted nanoplatforms.

Compared to MPBNPs-HED or free HED, the NEU@MPBNPs-HED group achieved better neuronal survival, motor recovery, and reduced glial scarring, as shown by BMS scores, CatWalk gait analysis, MEP amplitude, and immunofluorescence staining. These results underscore the therapeutic advantage of combining biomimetic targeting with responsive drug release for SCI repair.

Despite the promising therapeutic outcomes demonstrated by NEU@MPBNPs-HED, this study has several limitations. First, the in vivo evaluation was limited to a 14-day observation period, which may not fully capture long-term neuroregenerative effects or potential delayed toxicity. Second, while the neutrophil membrane facilitated lesion targeting, the precise molecular mechanisms underlying its homing behavior were not fully elucidated. Furthermore, large-scale extraction and purification of neutrophil membranes, while feasible in laboratory settings, may face hurdles in scalability and cost-effectiveness.And potential differences in immune recognition and response between rodents and humans must be carefully addressed to ensure translational safety and efficacy. Finally, although HED showed strong

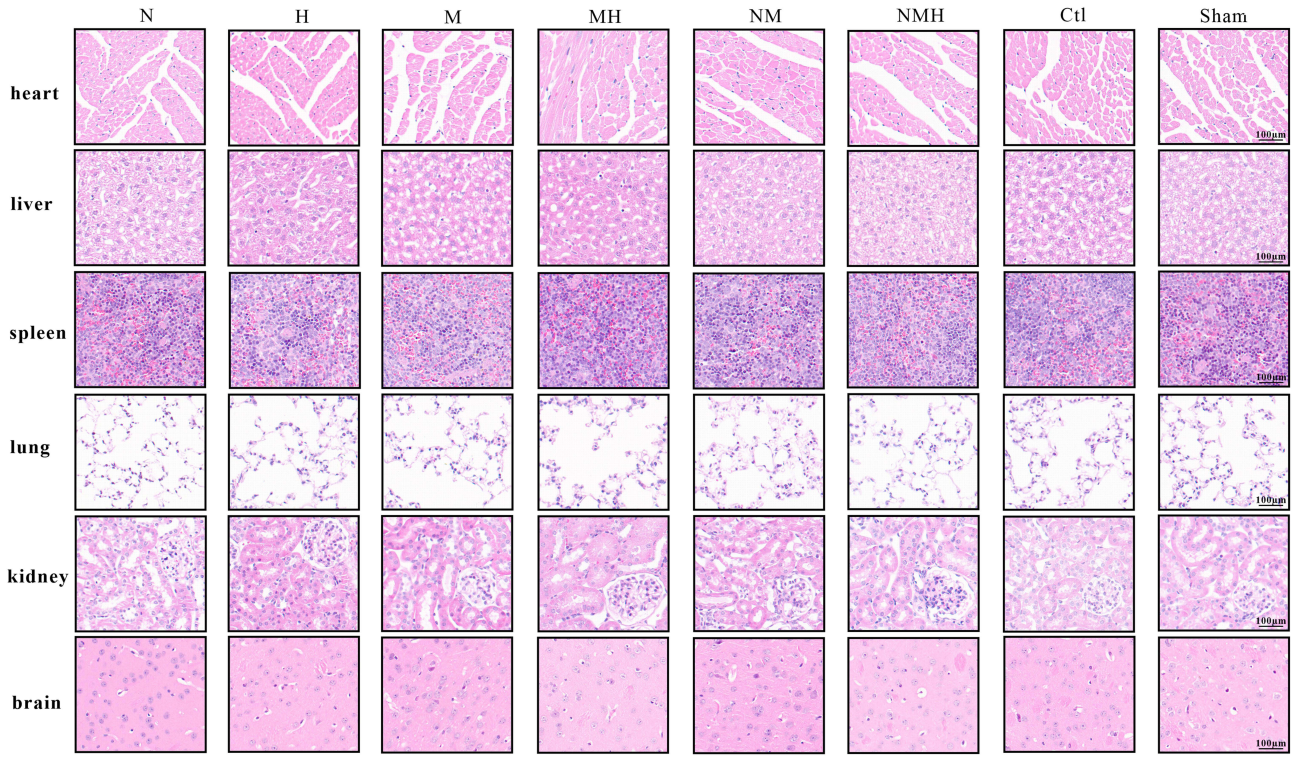

Figure 12 Histological images of heart, liver, spleen, lung, kidney, and brain samples from mice at 14 days after intravenous injection of PBS, NEUm, HED, MPBNPs, NEU@MPBNPs, MPBNPs-HED, and NEU@MPBNPs-HED. Ctl, control; N, NEUm; H, HED; M, MPBNPs; NM, NEU@MPBNPs; MH, MPBNPs-HED; NMH, NEU@MPBNPs-HED. Scale bar: 100 μm.

anti-apoptotic and antioxidant effects, its potential off-target actions and pharmacokinetics in the central nervous system warrant further investigation.

Conclusions

In our study, we developed a nanocomposite composed of neutrophil membrane (NEUm) nanovesicles encapsulating mesoporous Prussian blue nanoparticles (MPBNPs) loaded with Hederagenin (HED), termed as NEU@MPBNPs-HED. This nanocomposite demonstrated improved therapeutic effects compared to free HED and MPBNPs-HED for treating SCI. The NEUm nanovesicles allowed the nanocomposite to target the injury site, mimicking the natural behavior of neutrophils, which are attracted to areas of tissue damage. By camouflaging MPBNPs with NEUm, the nanocomposite evaded immune clearance, enabling it to effectively accumulate at the injury site. Additionally, MPBNPs exhibited efficient drug delivery and safety in vivo. Under the acidic conditions present at the injury site, the degradation of MPBNPs was accelerated, promoting the controlled release of HED and enhancing the therapeutic effect. This study demonstrated that NEU@MPBNPs-HED could improve tissue repair by regulating apoptosis and reducing further damage. The nanocomposite's safety, targeting ability, and efficacy make it a promising candidate for clinical application as a targeted drug delivery platform for SCI treatment, providing a foundation for future translational research.

Data Sharing Statement

The data are available from the corresponding author on reasonable request.

https://doi.org/10.2147/IJN.S547401

Ethics Approval

All animal procedures were approved by the Institutional Animal Care and Use Committee (IACUC) of The Second Qilu Hospital of Shandong University (Approval No. KYLL2024550) and conducted in compliance with the animal welfare guidelines as stipulated in the institutional guidelines (Directive 2010/63/EU in Europe) for the care and use of animals.

Acknowledgment

Shandong University Institute of Advanced Medical Research.

Author Contributions

All authors made a significant contribution to the work reported, whether that is in the conception, study design, execution, acquisition of data, analysis and interpretation, or in all these areas; took part in drafting, revising or critically reviewing the article; gave final approval of the version to be published; have agreed on the journal to which the article has been submitted; and agree to be accountable for all aspects of the work.

Funding

This work was supported by National Natural Science Foundation of China (No. 82220108005 and 92468205), Natural Science Foundation of Shandong Province (ZR2023ZD16), Taishan Scholar Program of Shandong Province-Pandeng Taishan Scholars (tspd20210320), and fund for education and training of The Second Qilu Hospital of Shandong University (No. 2023YP34).

Disclosure

The authors declare that there are no conflicts of interest regarding the publication of this paper.

References

1. Dolma S, Kumar H. Neutrophil, extracellular matrix components, and their interlinked action in promoting secondary pathogenesis after spinal cord injury. *Mol Neurobiol*. 2021;58(9):4652–4665. doi:10.1007/s12035-021-02443-5
2. Bourassa-Moreau É, Mac-Thiong JM, Li A, et al. Do patients with complete spinal cord injury benefit from early surgical decompression? Analysis of neurological improvement in a prospective cohort study. *J Neurotrauma*. 2016;33(3):301–306. doi:10.1089/neu.2015.3957
3. Kwon BK, Okon E, Hillyer J, et al. A systematic review of non-invasive pharmacologic neuroprotective treatments for acute spinal cord injury. *J Neurotrauma*. 2011;28(8):1545–1588. doi:10.1089/neu.2009.1149
4. Suberviola B, González-Castro A, Llorca J, Ortiz-Melón F, Miñambres E. Early complications of high-dose methylprednisolone in acute spinal cord injury patients. *Injury*. 2008;39(7):748–752. doi:10.1016/j.injury.2007.12.005
5. Anjum A, Yazid MD, Fauzi Daud M, et al. Spinal cord injury: pathophysiology, multimolecular interactions, and underlying recovery mechanisms. *Int J Mol Sci*. 2020;21(20):7533. doi:10.3390/ijms21207533
6. Kobayakawa K, Ohkawa Y, Yoshizaki S, et al. Macrophage centripetal migration drives spontaneous healing process after spinal cord injury. *Sci Adv*. 2019;5(5):eaav5086. doi:10.1126/sciadv.aav5086
7. Fleming JC, Norenberg MD, Ramsay DA, et al. The cellular inflammatory response in human spinal cords after injury. *Brain J Neurol*. 2006;129(Pt 12):3249–3269. doi:10.1093/brain/awl296
8. Okada S. The pathophysiological role of acute inflammation after spinal cord injury. *Inflamm Regen*. 2016;36(1):20. doi:10.1186/s41232-016-0026-1
9. Liou JT, Lee CM, Lin YC, et al. P-selectin is required for neutrophils and macrophage infiltration into injured site and contributes to generation of behavioral hypersensitivity following peripheral nerve injury in mice. *Pain*. 2013;154(10):2150–2159. doi:10.1016/j.pain.2013.06.042
10. Taoka Y, Okajima K, Uchiba M, et al. Role of neutrophils in spinal cord injury in the rat. *Neuroscience*. 1997;79(4):1177–1182. doi:10.1016/S0306-4522(97)00011-0
11. Farooque M, Isaksson J, Olsson Y. Improved recovery after spinal cord trauma in ICAM-1 and P-selectin knockout mice. *Neuroreport*. 1999;10(1):131–134. doi:10.1097/00001756-199901180-00024
12. Shen K, Li X, Huang G, et al. High rapamycin-loaded hollow mesoporous Prussian blue nanozyme targets lesion area of spinal cord injury to recover locomotor function. *Biomaterials*. 2023;303:122358. doi:10.1016/j.biomaterials.2023.122358
13. Andrabi SS, Yang J, Gao Y, Kuang Y, Labhasetwar V. Nanoparticles with antioxidant enzymes protect injured spinal cord from neuronal cell apoptosis by attenuating mitochondrial dysfunction. *J Control Rel*. 2020;317:300–311. doi:10.1016/j.jconrel.2019.12.001
14. He J, Qiao Y, Zhang H, et al. Gold-silver nanoshells promote wound healing from drug-resistant bacteria infection and enable monitoring via surface-enhanced Raman scattering imaging. *Biomaterials*. 2020;234:119763. doi:10.1016/j.biomaterials.2020.119763
15. Yang J, Zhai S, Qin H, Yan H, Xing D, Hu X. Corrigendum to "NIR-controlled morphology transformation and pulsatile drug delivery based on multifunctional phototheranostic nanoparticles for photoacoustic imaging-guided photothermal-chemotherapy" [Biomaterials 176 (2018) 1-12]. *Biomaterials*. 2019;217(217):119315. doi:10.1016/j.biomaterials.2019.119315
16. Gao A, Liao Q, Xie L, et al. Tuning the surface immunomodulatory functions of polyetheretherketone for enhanced osseointegration. *Biomaterials*. 2020;230:119642. doi:10.1016/j.biomaterials.2019.119642

17. Li J, Wei J, Wan Y, et al. TAT-modified tetramethylpyrazine-loaded nanoparticles for targeted treatment of spinal cord injury. *J Control Rel*. 2021;335:103–116. doi:10.1016/j.jconrel.2021.05.016
18. Gao X, Han Z, Huang C, et al. An anti-inflammatory and neuroprotective biomimetic nanoplatform for repairing spinal cord injury. *Bioact Mater*. 2022;18:569–582. doi:10.1016/j.bioactmat.2022.05.026
19. Kubelick KP, Emelianov SY. Prussian blue nanocubes as a multimodal contrast agent for image-guided stem cell therapy of the spinal cord. *Photoacoustics*. 2020;18:100166. doi:10.1016/j.pacs.2020.100166
20. Lin R, Liu L, Silva M, et al. Hederagenin protects PC12 cells against corticosterone-induced injury by the activation of the PI3K/AKT pathway. *Front Pharmacol*. 2021;12:712876. doi:10.3389/fphar.2021.712876
21. Shen Y, Teng L, Qu Y, et al. Hederagenin suppresses inflammation and cartilage degradation to ameliorate the progression of osteoarthritis: an in vivo and in vitro study. *Inflammation*. 2023;46(2):655–678. doi:10.1007/s10753-022-01763-5
22. Li Y, Dong J, Shang Y, Zhao Q, Li P, Wu B. Anti-inflammatory effects of hederagenin on diabetic cardiomyopathy via inhibiting NF-κB and Smads signaling pathways in a type-2 diabetic mice model. *RSC Adv*. 2019;9(45):26238–26247. doi:10.1039/C9RA02043H
23. Wang L, Zhao M. Suppression of NOD-like receptor protein 3 inflammasome activation and macrophage M1 polarization by hederagenin contributes to attenuation of sepsis-induced acute lung injury in rats. *Bioengineered*. 2022;13(3):7262–7276. doi:10.1080/21655979.2022.2047406
24. Liu J, Chen X, Xu L, et al. Neutrophil membrane-coated nanoparticles exhibit increased antimicrobial activities in an anti-microbial resistant K. pneumonia infection model. *Nanomedicine*. 2023;48:102640. doi:10.1016/j.nano.2022.102640
25. Baechler BL, Bloemberg D, Quadrilatero J. Mitophagy regulates mitochondrial network signaling, oxidative stress, and apoptosis during myoblast differentiation. *Autophagy*. 2019;15(9):1606–1619. doi:10.1080/15548627.2019.1591672
26. Youle RJ, Strasser A. The BCL-2 protein family: opposing activities that mediate cell death. *Nat Rev Mol Cell Biol*. 2008;9(1):47–59. doi:10.1038/nrm2308
27. Westphal D, Kluck RM, Dewson G. Building blocks of the apoptotic pore: how Bax and Bak are activated and oligomerize during apoptosis. *Cell Death Differ*. 2014;21(2):196–205. doi:10.1038/cdd.2013.139
28. Pistritto G, Trisciuoglio D, Ceci C, Garufi A, D'Orazi G. Apoptosis as anticancer mechanism: function and dysfunction of its modulators and targeted therapeutic strategies. *Aging*. 2016;8(4):603–619. doi:10.18632/aging.100934
29. Saunders TL, Windley SP, Gervinskas G, et al. Exposure of the inner mitochondrial membrane triggers apoptotic mitophagy. *Cell Death Differ*. 2024;31(3):335–347. doi:10.1038/s41418-024-01260-2
30. Fan L, Liu C, Chen X, et al. Exosomes-loaded electroconductive hydrogel synergistically promotes tissue repair after spinal cord injury via immunoregulation and enhancement of myelinated axon growth. *Adv Sci*. 2022;9(13):e2105586. doi:10.1002/advs.202105586
31. Lawrence T, Natoli G. Transcriptional regulation of macrophage polarization: enabling diversity with identity. *Nat Rev Immunol*. 2011;11(11):750–761. doi:10.1038/nri3088
32. Zhou K, Zheng Z, Li Y, et al. TFE3, a potential therapeutic target for spinal cord injury via augmenting autophagy flux and alleviating ER stress. *Theranostics*. 2020;10(20):9280–9302. doi:10.7150/thno.46566
33. Zheng G, Zhang H, Tail M, et al. Assessment of hindlimb motor recovery after severe thoracic spinal cord injury in rats: classification of CatWalk XT® gait analysis parameters. *Neural Regen Res*. 2023;18(5):1084–1089. doi:10.4103/1673-5374.355763
34. Yuan F, Peng W, Yang Y, et al. Endothelial progenitor cell-derived exosomes promote anti-inflammatory macrophages via SOCS3/JAK2/STAT3 axis and improve the outcome of spinal cord injury. *J Neuroinflammation*. 2023;20(1):156. doi:10.1186/s12974-023-02833-7
35. Xie L, Wu H, He Q, et al. A slow-releasing donor of hydrogen sulfide inhibits neuronal cell death via anti-PANoptosis in rats with spinal cord ischemia–reperfusion injury. *Cell Commun Signal*. 2024;22(1):33. doi:10.1186/s12964-023-01457-x
36. Zhu S, Ying Y, Ye J, et al. AAV2-mediated and hypoxia response element-directed expression of bFGF in neural stem cells showed therapeutic effects on spinal cord injury in rats. *Cell Death Dis*. 2021;12(3):274. doi:10.1038/s41419-021-03546-6